arXiv:1511.03084v1 [astro-ph.SR] 10 Nov 2015

The Complex Structure of Magnetic Field Discontinuities in the Turbulent Solar Wind

A. Greco[1], S. Perri[1], S. Servidio[1], E. Yordanova[2], and P. Veltri[1]

[1]*Dipartimento di Fisica, Università della Calabria, 87036 Rende (CS), Italy and*

[2]*Swedish Institute of Space Physics, Uppsala, Sweden*

(Dated: November 11, 2015)

Abstract

Using high resolution Cluster satellite observations, we show that the turbulent solar wind is populated by magnetic discontinuities at different scales, going from proton down to electron scales. The structure of these layers resembles the Harris equilibrium profile in plasmas. Using a multi-dimensional intermittency technique, we show that these structures are connected through the scales. Supported by numerical simulations of magnetic reconnection, we show that observations are consistent with a scenario where many current layers develop in turbulence, and where the outflow of these reconnection events are characterized by complex sub-proton networks of secondary islands, in a self-similar way. The present work establishes that the picture of "reconnection in turbulence" and "turbulent reconnection", separately invoked as ubiquitous, coexist in space plasmas.

In the past decades, spacecraft observations suggested that plasma turbulence shares many similarities with classical hydrodynamics. The power spectrum of magnetic field fluctuations as a function of frequencies f manifests an inertial range, with a Kolmogorov-like scaling $f^{-5/3}$ (see for example Ref. [1]). More recently, high resolution measurements revealed the presence of a secondary inertial sub-range, where the spectrum breaks down and exhibits a power index steeper than $-5/3$ [2, 3]. The characteristic scales at which this break-down occurs are given by the proton gyro-radius $\rho_p = v_{th,p}/\Omega_p$ (being $v_{th,p}$ the proton thermal speed and Ω_p the proton gyro-frequency) and/or the proton skin depth $d_p = c/\omega_{cp}$ (being c the speed of light and ω_{cp} the proton plasma frequency) [2, 4–6]. At these scales the dynamics could be mediated by kinetic-Alfvén fluctuations, whistler-like perturbations and coherent structures such as vortexes and current sheets [7].

The most narrow current sheets and filaments are present at electron scales, where turbulent energy eventually dissipates [8, 9], even if the energy-dissipation mechanisms in a weakly-collisional plasma such as the turbulent solar wind are far from being understood. Recent kinetic simulations [10–12] clearly demonstrate that dissipation in turbulence takes place at filamentary electron scale current sheets. Observations, however, are relatively ambiguous with respect to simulations because of measurement limitations (1D data spacecraft samplings). To elaborate a general picture of the processes that govern plasmas in the interplanetary medium as well as in laboratory experiments (e.g, [13]), it is therefore crucial to characterize the smallest scales with both observations and simulations.

One of the best candidate which may explain plasma energy dissipation on kinetic scales is magnetic reconnection. Magnetic reconnection is the change of topology of the magnetic field, with subsequent conversion of energy into flows, heat, and non-thermal effects. Usually, reconnection and turbulence have been studied as separate topics, but more recently it has been suggested that these effects might coexist [7, 9, 14]. Namely, reconnection of thin current sheets can take place in magnetohydrodynamics (MHD), as well as in plasma-kinetic models [10]. On a parallel path [15, 16], it has been proposed that the process of magnetic reconnection can be very efficient when turbulence develops “inside” the above thin current sheets. At very high Reynolds number, in fact, it is expected that these narrow current layers become strongly unstable, generating micro-plasmoids and secondary islands in a self-similar way [17, 18].

Here we investigate the coexistence of reconnection and turbulence in the space plasmas, inspecting the solar wind from large to small scales. The analysis of high resolution magnetic field

measurements will be supported by numerical simulations. The results obtained merge the picture of "reconnection-in-turbulence", where large scale energy containing structures reconnect producing layers at scales on the order of the proton skin depth, with the picture of "turbulent-reconnection", where turbulence develops inside the outflows of the above current sheets, at scales on the order of (and much smaller than) the proton skin depth.

The data analyzed are taken in the pristine, undisturbed solar wind from the Cluster 4 spacecraft on 2007 January 20, 12:00-14:00 UT. Following [19], the FGM and the STAFF data in burst mode (sampling frequencies 67 and 450 vec/sec, respectively) are combined by low-passing FGM data and high-passing STAFF data using a cutoff frequency of 1 Hz. In this sampling, the solar wind bulk speed is $V_{\rm sw} \sim 600$km/s, the mean magnetic field (averaged over the entire data set) is $B_0 \sim 4$ nT (see also Table 1 in Yordanova et al. [19]). In terms of characteristic plasma scales, the proton Larmor radius is $\rho_p \sim 193$ km, the proton inertial length $d_p \sim 163$ km, the electron Larmor radius $\rho_e \sim 3.67$ km and the electron inertial length $d_e \sim 3.75$ km. The magnetic field power spectral densities of the magnetic field components in Geocentric-Solar-Ecliptic (GSE) reference frame are shown in Figure 1. A well defined spectral break at ~ 0.5Hz is observed, separating the Kolmogorov-like inertial range with spectral slope -1.5 from the steeper high frequency range. The short vertical lines indicates the Doppler shifted proton (electron) gyroradii $f_{\rho\ p(e)} = V_{\rm sw}/2\pi\rho_{p(e)}$ and inertial lengths $f_{d\ p(e)} = V_{\rm sw}/2\pi d_{p(e)}$. The change in the slope of the power spectrum at frequencies higher than the proton gyro-frequency indicates a change in the nature of the turbulent cascade with possible plasma-kinetic effects at work [2, 13, 20]. However, it is not clear whether the breaking frequency is due to Larmor radius or to proton skin depth effects [21].

Beside the spectral properties, plasma turbulence is spatially characterized by intermittent structures (bursty in space) [8, 22–24]. These structures can be classified in several ways [25], but they are generally strong inhomogeneities of the magnetic field [26, 27]. To trace these abrupt spatial changes of the magnetic field, we use the Partial Variance of Increments (PVI), which measures the "spikiness" of the signal relative to a Gaussian value and is directly connected to the intensity of the current [28]. The PVI time series is defined in terms of the magnetic field increment vector $\Delta\mathbf{B}(t,\tau) = \mathbf{B}(t+\tau) - \mathbf{B}(t)$ [29]:

$$PVI(t,\tau) = \frac{|\Delta\mathbf{B}(t,\tau)|}{\sqrt{\langle|\Delta\mathbf{B}(t,\tau)|^2\rangle}} \tag{1}$$

where the average is over a suitably large trailing sample computed along the time series and τ is

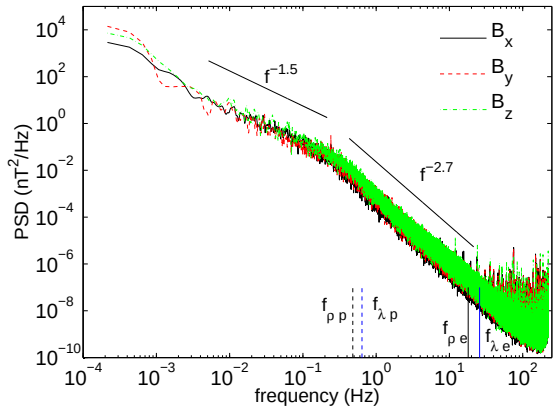

FIG. 1. (Color online) Power spectral density (PSD) of the magnetic field. The spectral slopes of the inertial range and of the high frequency range are displayed. Characteristic plasma frequencies are reported with vertical lines (see text).

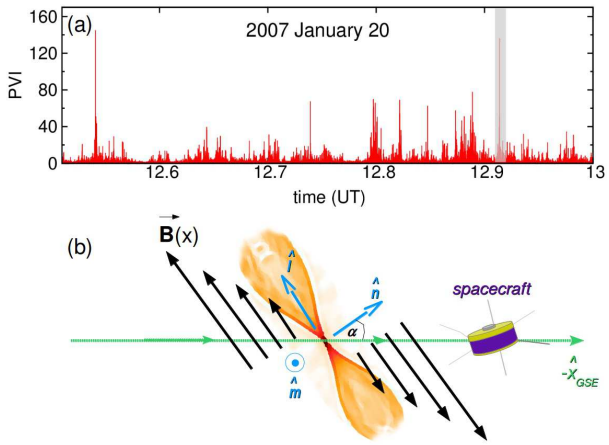

FIG. 2. (Color online) (a) PVI signal computed for $\tau = 0.022$ s. (b) Cartoon of a current layer crossing the spacecraft, which possibly corresponds to a peak in the PVI. The axes of the minimum variance reference system $(\hat{\mathbf{l}}, \hat{\mathbf{m}}, \hat{\mathbf{n}})$ are also depicted.

the time lag. For this study we compute PVI on inertial scales from $\tau = 15$ s to 1 s, and on kinetic sub-proton scales ranging from $\tau = 0.7$ s to 0.022 s. The smallest time separation used correspond to a frequency of 45 Hz, where the signal-to-noise ratio is still high. The PVI series, computed for $\tau = 0.022$ s, is reported in Figure 2-(a) for a portion of the data-set. The signal, as it can be seen, displays a strongly intermittent character, typical of turbulence.

In order to characterize the most abrupt events, a set of structures with PVI amplitude above a given threshold can be defined. Once these structures have been localized, the magnetic filed has

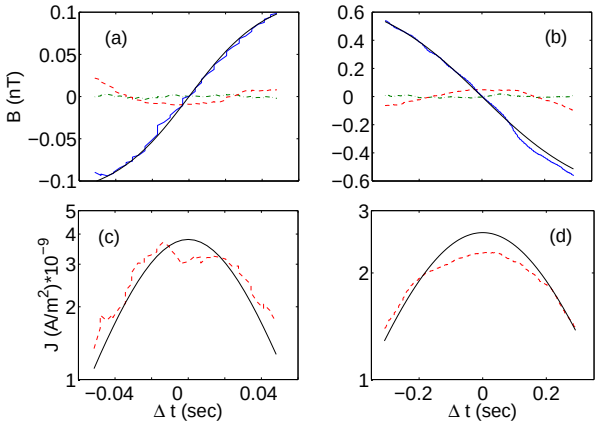

FIG. 3. (Color online) (a) Magnetic field, in the local minimum variance frame, in a discontinuity at electron (a) and sub-proton (b) scales. B_l is reported with solid (blue), B_n with dot-dashed (green), and B_m with dashed (red) line. The thick (black) line represents the Harris profile with $\lambda = 3d_e$ (a) and $55d_e$ (b). (c) and (d) report the surrogate current density (red-dashed) for the discontinuities in (a) and (b), respectively, together with the Harris current (black solid).

been rotated in the local minimum variance reference frame [8, 30], defined by the basis $(\hat{\mathbf{l}}, \hat{\mathbf{m}}, \hat{\mathbf{n}})$. As reported in Figure 2-(b), $\hat{\mathbf{l}}$ is the unit vector along the maximum, $\hat{\mathbf{m}}$ along the medium, and $\hat{\mathbf{n}}$ is along the minimum-variance direction. Note that in this reference frame the structures can be classified in different ways: tangential or rotational discontinuities, magnetic holes and so on [31] (a detailed classification of magnetic discontinuities is beyond the scope of the Letter). We further estimate the current density vector $\boldsymbol{J} = \boldsymbol{\nabla} \times \boldsymbol{B}/\mu_0$ within those structures. From a single-satellite sampling, the only two components of $\boldsymbol{J}$ that can be estimated are J_y and J_z (multispacecraft techniques are not applicable in this analyzed period). These components have been computed via the magnetic field differences along GSE x direction, in the limit of small τ. Structures showing the minimum variance axis $\hat{\mathbf{n}}$ almost parallel to x axis have been selected. First, we impose that the angle between $\hat{\mathbf{n}}$ and x is $\alpha < 8^\circ$. Second, we restrict to layers with the minimum variance component $B_n \sim B_m \sim 0$. This configuration restricts the analysis of the current to the cases reported in the cartoon of Figure 2-(b). These constraints ensure that the above surrogate computed from the Cluster 4 data, is very close to the actual current density.

The strongest current layers detected by the PVI method, at time lags that range from inertial to sub-proton time scales seem to have a self-consistent shape, resembling equilibrium solutions of

both fluid-like and kinetic plasmas. The simplest analytical model that could represent thin current layers on kinetic scales is the well-known Harris sheet [32], which is widely used to describe a plasma sheath confined between two regions of oppositely directed magnetic field. It is a kinetic equilibrium and the earliest exact analytical solution of the Vlasov equation. Under some assumptions the magnetic field follows a 1D hyperbolic-tangent profile. Figure 3 shows two examples of 1D current sheets, detected by PVI method, in their local minimum variance reference frame. The time duration is $\Delta t \sim 0.1$ s (a) and $\Delta t \sim 0.7$ s (b), that correspond to 60 km and 420 km along x, respectively, assuming the validity of the Taylor frozen-in hypothesis. The maximum variance component B_l performs a smooth, large amplitude rotation, while $B_m \sim B_n \sim 0$. Note that B_m, albeit very small, displays a multi-polar signature, typical of solar wind reconnection exhausts [33]. The best fits from the Harris model $B = B_0 tanh(x/\lambda)$, where $x = V_{\rm sw} t$ and λ is the half-thickness of the layer, are also compared in the same figures, indicating very good agreement with the plasma equilibrium theory. The value of λ is $\sim 3d_e$ for the current sheet on the left and $\sim 55d_e$ for that on the right. In the bottom panels, the magnitude of the (partial) current density $J = \sqrt{J_y^2 + J_z^2}$ is shown for the same structures, comparing the profile with the Harris expectation $J \sim (B_0/\lambda)\cosh^{-2}(x/\lambda)$.

The Harris profile persists from inertial down to electron scales in a self similar way. Many of them are isolated, other seem to cluster, being embedded in larger scales discontinuous layers. In order to quantify this cross-scale connection, we performed a multi-dimensional intermittency analysis, computing the full PVI as a function of both scales and positions. Figure 4 represents this "scalogram" of the PVI series, taken in a sub-interval of the original data-set, where time t has been converted in space s and the time lag τ in the spatial scale Δs, both normalized to the proton inertial length d_p. The two-dimensional contour clearly shows high values of PVI (current) at large scales that connect down to kinetic scales, at wavelengths smaller than the proton skin depth. This connection is very interesting and somehow complex, being an ubiquitous manifestation of intermittency in plasma turbulence. The most interesting feature of the plot is the "ramification" of the current, following large scale shears, going down to kinetic scales: discontinuities on the order of the proton skin depth (or bigger) seem to "break up" into smaller sub-proton structures. These nested structures are characterized by high values of the current. Some of these are the 1D current sheets depicted in Figure 3, some other might be related to substructures of the outflows layer, as we will investigate below.

It has been established, both from observations [34, 35] and from theory and simulations [14],

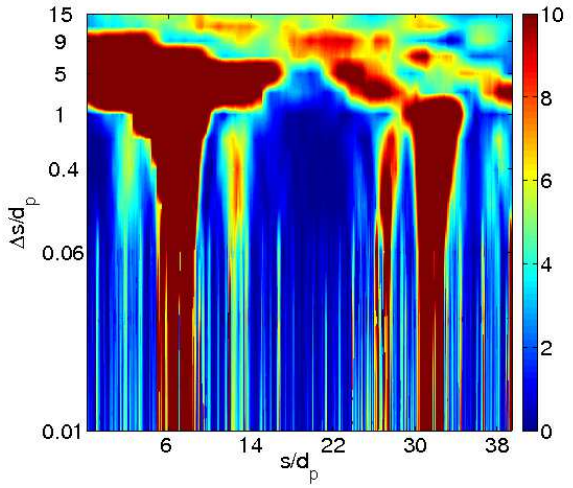

FIG. 4. (Colo online) PVI intensity as a function of space and scale in units of the proton inertial length, computed from Cluster 4. Large scale layers break down into thinner sub-proton magnetic structures.

that turbulence provides a broad distribution of reconnection events, and that at very high Reynolds number these micro-structures undergo secondary instabilities, producing turbulent outflows with secondary structures embedded [36]. In order to capture the magnetic reconnection at scales on the order of the proton skin depth, we perform direct numerical simulations of two-dimensional (2D) compressible Hall MHD. The use of Hall MHD is important in order to understand the minimal physics of the plasma turbulent cascade, as well as the basic physics of reconnection that might be at work in the above intermittent events. We perform the simulation in a periodic geometry, in a x-y plane, using for the initial conditions a double-periodic Harris sheet. The current sheet is modeled such that at the initial time, in each current layer, $B_x(y) \sim tanh(y/\lambda)$, with $\lambda \sim 2d_p$, and sustained by pressure balance. The code makes use of a spectral algorithm, as described in [37], and conserves with high accuracy the global invariants of the system.

The double-periodic current sheets are perturbed with broad-band noise, with an amplitude of $\sim 5\%$, undergoing therefore magnetic reconnection. After the initial evolution, a fully nonlinear steady state of magnetic reconnection is reached, as shown in Figure 5-(a), where the current density together with the in-plane magnetic field lines are reported. Current sheets become thinner than the proton skin depth, and strong outflows are generated, feeding large scale magnetic islands. At this stage of the simulation, we mimic a satellite-like sampling, taking advantage of the periodic boundary conditions. At the peak of the nonlinear activity, where secondary islands and micro-current sheets as well as plasmoid have been formed (especially in the exhausts) [33, 38], one

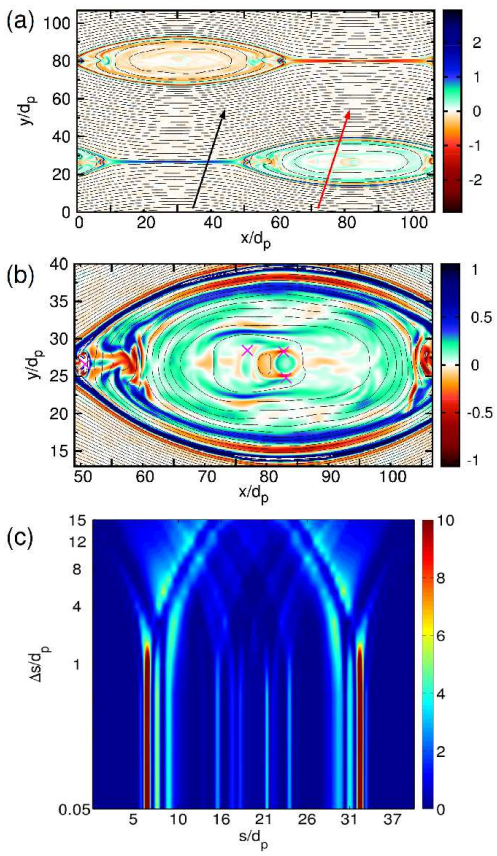

FIG. 5. (Color online) (a) Shaded contour of the current density with in-plane magnetic field lines (black). Arrows indicate two different possible spacecraft crossings. (b) Zoom into the outflow region, showing its complex structure, with secondary $\times$-points (magenta symbols). (c) Joint-PVI, as in Figure 4, for an outflow crossing. The cross-scale coupling at sub-proton scales is evident.

can interpolate the magnetic field through a satellite that flows through turbulence, simulating the effect of 1D solar wind sampling. These imaginary trajectories are pictorially reported with arrows in Figure 5-(a). Each trajectory has been chosen to form an oblique angle of 80° with x, cutting the current sheets almost perpendicularly. Obviously, even in a very basic and idealized scenario where only current sheets are present, there are several possibility for crossing the reconnecting layer, at different angles, and different distances from the $\times$-point. Based on simple arguments on the size of the structures (small current sheets and big growing islands), the most probable region are the outflows [39]. As reported in Figure 5-(b), the structure of the outflows is very complex, where different current layers, plasmoids, and secondary current sheets are formed. Inside this structure, indeed, one can detect several secondary $\times$-points, where reconnection is occurring in a self-similar way.

Finally, in order to establish a direct connection with observations, we computed $PVI(s, \Delta s)$ on an oblique path which crosses the current sheets in the double periodic simulation of Figure 5-(a). As in the solar wind, the imaginary satellite eventually crosses the main current layer, and a cross-scale effect in the joint-PVI is observed. In particular, as reported in Figure 5-(c), when the sampling is along the large outflow, several sub-structures are found in the turbulent layer, down to sub-proton scales. Obviously, when the scales approach the electron skin depth, other numerical models need to be taken into account, since kinetic-electron physics may play a major role [10]. Current "fragmentation" is met along the direction perpendicular to initial current sheets, similarly to the scenario observed in solar wind turbulence. Indeed, in plasma turbulence magnetic reconnection is a common feature, characterizing the strongest intermittent current sheets. In these current layers, systematically, the sheets break into smaller ones giving rise to a complex network of secondary structures. These sub-proton structures are here detected with the PVI technique, and the scenario is further supported by simulations.

In summary, using Cluster high resolution data, we investigated the structure of thin current sheets that populate the turbulent solar wind. The following picture emerges for the solar wind: the turbulent cascade naturally forms current sheets at several scales, down to the proton skin depth. Approaching smaller scales, a current "fragmentation" process arises, producing Harris-like layers down to scales comparable with the electron skin depth. These processes have been described with the support of 2D compressible Hall MHD simulations of magnetic reconnection, where complex outflows are produced, showing that the cross-scale structure of the current sheets, where secondary islands are embedded in the outflows, is consistent with the observations. The concepts of reconnection-in-turbulence and turbulent-reconnection, that have been invoked as separate paradigms of plasma physics in the past decades, are here found to be two synergistic processes of space plasmas.

E. Y. received funding from EC FP7 ([7/2007-2013]) under grant agreement No. 313038/STORM.

[1] R. Bruno and V. Carbone, *Liv. Rev. Solar Phys.* **10**, 2 (2013).

[2] F. Sahraoui, M. L. Goldstein, P. Robert, and Y. V. Khotyaintsev, Phys. Rev. Lett. **102**, 231102 (2009).

[3] O. Alexandrova, J. Saur, C. Lacombe, A. Mangeney, J. Mitchell, S. J. Schwartz, and P. Robert, Phys. Rev. Lett. **103**, 165003 (2009).

[4] S. D. Bale, P. J. Kellogg, F. S. Mozer, T. S. Horbury, and H. Reme, Phys. Rev. Lett. **94**, 215002 (2005).

[5] F. Sahraoui, M. L. Goldstein, G. Belmont, P. Canu, and L. Rezeau, Phys. Rev. Lett. **105**, 131101 (2010).

[6] Y. Narita, S. P. Gary, S. Saito, K. H. Glassmeier, and U. Motschmann, Geophys. Res. Lett. **38**, L05101 (2011).

[7] K. T. Osman, W. H. Matthaeus, J. T. Gosling, A. Greco, S. Servidio, B. Hnat, S. C. Chapman, and T. D. Phan, Phys. Rev. Lett. **112**, 215002 (2014).

[8] S. Perri, M. L. Goldstein, J. C. Dorelli, and F. Sahraoui, Phys. Rev. Lett. **109**, 191101 (2012).

[9] M. L. Goldstein et al., J. Plasma Phys. **81**, 1 (2015).

[10] H. Karimabadi et al., Phys. Plasmas **20**, 012303 (2013).

[11] C. T. Haynes, D. Burgess, and E. Camporeale, Astrophys. J. **783**, 38 (2014).

[12] M. Wan, W. H. Matthaeus, V. Roytershteyn, H. Karimabadi, T. Parashar, P. Wu, and M. Shay, Phys. Rev. Lett. **114** , 175002 (2015).

[13] D. A. Shaffner and M. R. Brown, Astrophys. J. **811**, 61 (2015).

[14] S. Servidio, W. H. Matthaeus, M. A. Shay, P. A. Cassak, and P. Dmitruk, Phys. Rev. Lett. **102**, 115003 (2009).

[15] W. H. Matthaeus and S. L. Lamkin, Phys. Fluids **29**, 2513 (1986).

[16] A. Lazarian and E. Vishniac, Astrophys. J. **517**, 700 (1999).

[17] G. Lapenta, Phys. Rev. Lett. **100**, 235001 (2008).

[18] R. Samtaney, N. F. Loureiro, D. A. Uzdensky, A. A. Schekochihin, and S. C. Cowley, Phys. Rev. Lett. **103**, 105004 (2009).

[19] E. Yordanova, S. Perri, L. Sorriso-Valvo, and V. Carbone, Europhys. Lett. **110**, 19001 (2015).

[20] O. Alexandrova, C. H. K. Chen, L. Sorriso-Valvo, T. S. Horbury, and S. D. Bale, Space Sci. Rev. **178**, 101 (2013).

[21] D. Telloni, R. Bruno, and L. Trenchi, Astrophys. J. **805**, 46 (2015).

[22] P. Veltri, Plasma Phys. Contr. Fusion, **41**, 787 (1999).

[23] K. H. Kiyani, S. C. Chapman, Yu. V. Khotyaintsev, M. W. Dunlop, and F. Sahraoui, Phys. Rev. Lett. **103**, 075006 (2009).

[24] R. Bruno, V. Carbone, P. Veltri, E. Pietropaolo, and B. Bavassano, Planet. Space Sci. **49**, 1201 (2001).

[25] P. Veltri, G. Nigro, F. Malara, V. Carbone, and A. Mangeney, Nonlinear Process. Geophys. **12**, 245 (2005).

[26] L. F. Burlaga and N. F. Ness, Can. J. Phys. Suppl. **46**, 962 (1968)

[27] B. T. Tsurutani and E. J. Smith, J. Geophys. Res. **84**, 2773 (1978)

[28] S. Donato, A. Greco, W. H. Matthaeus, S. Servidio, and P. Dmitruk, J. Geophys. Res. **118**, 7 (2013).

[29] A. Greco, P. Chuychai, W. H. Matthaeus, S. Servidio, and P. Dmitruk, Geophys. Res. Lett. **35**, 19111 (2008).

[30] B. U. O. Sonnerup and L. J. Cahill, J. Geophys. Res. **72**, 171 (1967).

[31] A. Greco and S. Perri, Astrophys. J. **784**, 163 (2014).

[32] E. G. Harris, Nuovo Cimento **23**, 115 (1961).

[33] S. Eriksson et al., Astrophys. J. **805**, 43 (2015).

[34] A. Retinò, D. Sundkvist, A. Vaivads, F. Mozer, M. André, and C. J. Owen, Nat. Phys. **3**, 236 (2007).

[35] D. Sundkvist, A. Retinò, A. Vaivads, and S. D. Bale, Phys. Rev. Lett. **99**, 025004 (2007).

[36] M. Wan, S. Oughton, S. Servidio, and W. H. Matthaeus, Phys. Plasmas **16**, 080703 (2009).

[37] S. Ghosh, M. Hossain, and W. H. Matthaeus, Comput. Phys. Commun. **402**, 74 (1993).

[38] G. Lapenta, S. Markidis, M. V. Goldman, and D.L. Newman, Nat. Phys., DOI: 10.1038/NPHYS3406 (2015).

[39] J. T. Gosling, Space Sci. Rev. **4172**, 187 (2012).